Design and fabrication of porous chitosan scaffolds with tunable structures and mechanical properties

Yongxiang Xu[a], Dandan Xia[a], Jianmin Han[a], Shenpo Yuan[a], Hong Lin[a,*], Chao Zhao[b,*]

[a] Department of Dental Materials, Peking University School and Hospital of Stomatology, National Engineering Laboratory for Digital and Material Technology of Stomatology, Beijing Key Laboratory of Digital Stomatology, Beijing, China
[b] Department of Chemical and Biomolecular Engineering, The University of Akron, Akron, OH, USA

ARTICLE INFO

ABSTRACT

Chitosan-based porous scaffolds are of great interest in biomedical applications because of their biodegradability and biocompatibility. However, the poor mechanical properties of these scaffolds hinder their broad utility. In the present study, a novel compression method was developed to fabricate chitosan scaffolds with high mechanical strength and tuneable topography, based on the ionic strength and pH-dependent solubility of chitosan. When the compressive ratio increases from 1 to 8, the compressive elastic modulus of the scaffold increases from 5.2 kPa to 520 kPa and the porosity decreases from 94.1% to 82.5%. Furthermore, the number of human adipose-derived stem cells adhering to the scaffolds increases as the compressive ratio increases, owing to the high density of the chitosan fibres. This method does not require external cross-linker agent, sophisticated instrumentation and/or technical proficiency and could be extended to other polysaccharides.

1. Introduction

Tissue engineering is a promising approach to enhance or replace damaged biological tissues, using cells growing on biocompatible scaffolds (Langer & Vacanti, 1993). The structure and properties of the scaffolds play a pivotal role in tissue engineering because they provide a three-dimensional structure for not only the adhesion, differentiation, and proliferation of cells, but also the exchange of nutrients and metabolic waste (Hutmacher, 2000). Regardless of tissue type, many general requirements are important when designing and fabricating a scaffold for use in tissue engineering: (1) biocompatibility and biodegradability of the biomaterials; (2) mechanical properties appropriate to the anatomical site; (3) architecture that mimics the extra cellular matrix, including appropriate porosity and an interconnected pore structure (Ma, 2004; O'Brien, 2011).

Polysaccharide-based scaffolds are widely used in tissue regeneration because of their excellent biodegradability, biocompatibility, and bioactivity (Khan & Ahmad, 2013; Oh, Ko, Lu, Kawazoe, & Chen, 2012). Chitosan is a compound derived from the partial deacetylation of natural chitin and can be fabricated to a scaffold via covalent/ionic cross-linking, complexation with another polymer or aggregation after CS grafting and so on. Furthermore, it can be used to generate physical microcrystalline and chain-entanglement networks after simple treatment in alkaline, without the requirement for external cross-linker. Numerous methods have been proposed for fabrication of scaffolds with well-defined structures and properties from chitosan solutions, such as lyophilization, porogen leaching, micro-templating, and 3D-printing (Choi, Xie, & Xia, 2009; Geng et al., 2005; Li et al., 2014; Madihally & Matthew, 1999).

Nevertheless, the low mechanical strength of chitosan scaffolds hinders their broad utility for tissue engineering, especially for load-bearing usage (Subramanian & Lin, 2005). Previous research efforts improved the mechanical properties and structures of chitosan-based scaffolds through chemical cross-linking and/or formation of composites with reinforcement agents, synthetic polymers, or another natural polymer (Huang, Onyeri, Siewe, Moshfeghian, & Madihally, 2005; Sadeghi et al., 2016; Zhang et al., 2008). These chitosan-based scaffolds have significantly better mechanical strength and elastic moduli. However, cross-linkers and additives can potentially alter the biological properties of chitosan scaffolds, and unfavourable toxic effects on cells have been reported (Albanna, Bou-Akl, Blowytsky, & Matthew, 2012).

Without external cross-linking agent, the mechanical strength of chitosan scaffolds was improved by other methods, such as altering the concentrations or the pH of the chitosan solution (Bhattarai, Gunn, & Zhang, 2010; Jana, Florczyk, Leung, & Zhang, 2012), changing the solvent system (Sun, Li, Nie, Wang, & Qiao ling, 2013; Wang, Nie,

Qin, Hu, & Tang, 2016) or heat-compressing the lyophilized scaffold (Campbell, Wiesmann, & McCarthy, 2012; Farrugia et al., 2014). Nevertheless, these methods were strictly limited by the low solubility and high viscosity of chitosan and difficult to control the structure and properties of chitosan scaffolds. Thus, novel methods to improve the mechanical properties of polysaccharide scaffolds are urgently needed to facilitate improvements in tissue bioengineering.

In the present study, based on the ionic strength-dependent and pH-dependent solubility of chitosan, a novel compression method was developed to fabricate porous chitosan scaffolds to achieve high mechanical strength and tuneable topography. Moreover, this method does not require external cross-linking agents, sophisticated instrumentation, and/or technical proficiency, and could be conveniently scaled up for mass production. The effects of preparation conditions on the properties of the scaffold were studied and the mechanism was analysed. Although this method was only applied to chitosan in the present research, it could be extended to other polysaccharides.

2. Material and methods

2.1. Materials

Chitosan ($\overline{M}_\eta = 187\,\text{kDa}$, de-acetylation = 89.8%), acetic acid, PBS, sodium chloride (NaCl), sodium hydroxide (NaOH), and other agents were purchased from Sinopharm Chemical Reagent Beijing Co., Ltd., China. All chemicals were of analytical grade and were used without further purification. Human adipose-derived stem cells (*hASCs*) were purchased from ScienCell (San Diego, CA, USA).

2.2. Preparation of chitosan scaffolds

Chitosan scaffolds were fabricated utilizing a two-step method. Chitosan was dispersed in de-ionized water and a stoichiometrically equivalent amount of acetic acid was added. After complete dissolution, the solution was left to stand for 24 h without stirring for degassing at 4 °C. The solution was then injected into a cylindrical mould (φ 12.0 × 12.0 mm) and frozen at −20 °C for 24 h. The frozen chitosan was immersed in a saturated NaCl solution at −20 °C for 48 h and then stored at 23 °C for 48 h to prepare scaffold-I. Scaffold-I was compressed radially at different ratios ($R = h_0/h_1$) and then immersed in a neutralization (NaOH + NaCl) solution under compression to fabricate scaffold-II. Finally, all the samples were washed three times with de-ionized water and then stored in phosphate buffered saline (1 × PBS, pH = 7.4) for 24 h to mimic pseudo-physiological conditions before testing.

2.3. Structure of chitosan scaffolds

Images of scaffolds forming under various conditions were captured using a digital camera (EOS 5D Mark II, Canon, Tokyo, Japan). Furthermore, the liquid-nitrogen fracture surfaces of the scaffolds were coated by *Au* film with an approximate thickness 20 nm and then characterized using a scanning electron microscope (SEM, EVO 18, Zeiss, Oberkochen, Germany).

2.4. Physico-mechanical characterization of chitosan scaffolds

2.4.1. Pore diameter (D) and porosity (P)

The pore diameter (*D*) and porosity (*P*) of scaffold-II were analysed by a mercury intrusion porosimeter (Autopore IV 9500, Micromeritics, GA, USA). The porosity of scaffold-I was calculated according to the volume of scaffold-I and the porosity of scaffold-II, which was prepared using the same sample of scaffold-I. The contact angle of mercury on chitosan was 130°, and mercury was filled progressively with filling pressure of 1.2 kPa to 414 MPa.

2.4.2. Young's modulus (E)

The mechanical properties, i.e., *E*, of the chitosan scaffolds were determined by compression testing at a rate of 5.0 mm/min at a temperature of 23 ± 2 °C, using a universal material testing machine (model 5543A, Instron, Norwood, MA, USA).

2.5. Influence of preparation conditions on chitosan scaffolds

The saturated NaCl solution was used to prepared scaffold-I because the melting point of frozen chitosan samples at 20 mg/ml is −16 °C, and low-concentration NaCl solutions would freeze at this temperature. The effect of the NaCl concentration (C_{NaCl}) was studied after scaffold-I was prepared.

The *R* value is a key factor affecting the structure and properties of chitosan scaffolds. The effect of the concentration and composition of the NaOH solution was further studied.

2.6. pH-responsive properties

The stimulus-responsive properties of the scaffold were studied. Each sample was immersed in 10 ml 1 × PBS solution with various pH values (pH = 3.0, 5.5, 7.4, and 9.0) for 24 h and the changes in *E* and *P* were measured.

2.7. Cytotoxicity assays

The cytotoxicity of the scaffolds was evaluated using extracts and L929 fibroblast cells (ATCC, Manassas, VA, USA) following ISO 10993-5:2001 standards. The test scaffold extract was prepared with 0.5, 1.0, and 1.5 mg of chitosan in 1 ml of minimum essential medium (MEM) at 37 °C for 24 h. The blank culture medium and 10% DMSO were used as negative and positive controls, respectively. The optical intensity was measured at a wavelength of 570 nm using a microplate reader (Model 680, Bio-Rad, USA). The cytotoxicity of the scaffold was expressed as % cell viability, which was calculated from the ratio between the number of cells treated with the polymer solutions and that of non-treated cells (control).

### 2.8. Proliferation and adhesion of immobilized cells

The hASCs were cultured in Dulbecco's modified eagle medium supplemented with 10% fetal bovine serum and 100 IU/ml penicillin-streptomycin. The medium was changed every 2 days. At 80–90% confluence, the hASCs were detached with 0.25% trypsin/ethylene-diaminetetraacetic acid. The cells from 3 to 5 passages were used in the following studies. hASCs (1.0×10^5 cells/well) were seeded onto experimental scaffolds in 48-well plates and incubated at 37 °C in a humidified atmosphere with 5% CO_2. Scaffolds were fixed in 4% paraformaldehyde and 0.1% Triton X-100 at 23 °C. Scaffolds were then washed three times with 1 × PBS and incubated with fluorescein isothiocyanate (FITC)-labelled phalloidin and 6-diamidino-2-phenylindole (DAPI) solution at 37 °C. Fluorescence images of stained constructs were obtained using a confocal laser scanning microscope (Carl Zeiss Microimaging, Oberkochen, Germany) using wavelengths of 488 nm (green, FITC-labelled phalloidin) and 405 nm (blue, DAPI-labelled).

3. Results and discussion

3.1. Fabrication process of the chitosan scaffolds

Scheme 1 illustrated the fabrication process and mechanism of chitosan scaffold. The chitosan solution was first frozen in customized mould with a desired shape. Scaffold-I was fabricated basing on the ionic strength-dependent solubility of chitosan. After compression, scaffold-II was formed from the neutralization of $-NH_3^+$ to $-NH_2$.

The morphologies of the frozen chitosan solution, chitosan scaffold-
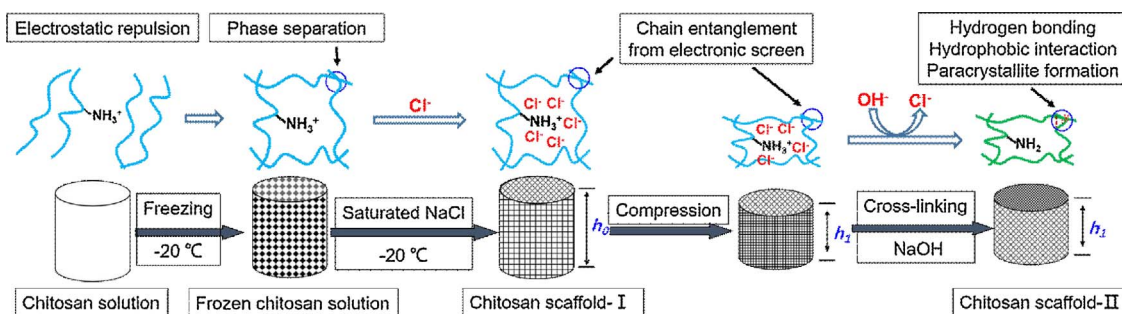
Scheme 1. Schematic illustration of the process and mechanism for fabrication of chitosan scaffolds.
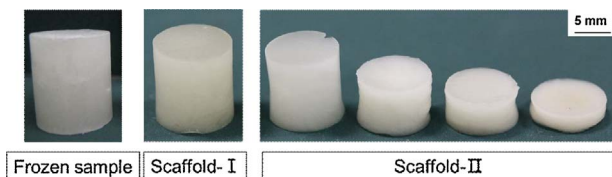

Fig. 1. Digital images showing the morphologies of frozen chitosan solution, chitosan scaffold-I, and scaffold-II.

I, and scaffold-II are shown in Fig. 1. The original shape of the frozen sample determined the shape of the chitosan scaffolds. The structure and properties of scaffold-II were changed during the compressing process.

3.2. Microstructure of the chitosan scaffolds

The fracture surface of the scaffolds was observed using SEM after thorough washing of the sample with de-ionized water and lyophilizing. An open-pore microstructure with a high degree of interconnectivity was observed in scaffold-I and scaffold-II after lyophilization, regardless of the compression value (Fig. 2). NaCl granular crystal was visible in every pore of scaffold-I. As R increased, the pore size of scaffold-II decreased, especially along the direction of compression.

3.3. Effect of preparation conditions on scaffold-I

The ionic strength-dependent solubility of chitosan was used to fabricate scaffold-I. The primary aliphatic amines (pKa = 6.3) of chitosan was protonated in acetic acid solution ($-NH_2$ to $-NH_3^+$), which causes electrostatic repulsion between the polymer chains, rendering the corresponding chitosan salt soluble (Bhattarai et al., 2010). When the frozen samples were immersed in a saturated NaCl solution at -20 °C, the ice inside the samples was gradually replaced by the NaCl solution; the high ionic strength (Cl^-) electronically screened the $-NH_3^+$, which induced screening of the electrostatic repulsion between the polymer chains, therefore favouring physical junctions inside the entangled chain (Yang, Wang, Yang, Shen, & Wu, 2016).

Fig. 3A shows the effect of the C_0 of the chitosan solution on E and P. As C_0 increased from 10 mg/ml to 40 mg/ml, density of junction points of scaffold-I increased. E increased from 1.2 kPa to 9 kPa, and P decreased from 97.2% to 95.8%. The compressive stress–strain curves of scaffold-I are illustrated in. The chitosan scaffold showed three distinct regions in compressive stress–strain plots (Fig. 3B). In the first region, the response was linear and the elastic modulus was calculated from the slope of this region. In the second region, the strain–stress response resulted from the collapsed scaffold and, in this region, the slope of the curve decreased significantly. Compressive mechanical strength was determined from the onset of the second region. Further compression induced densification of the scaffold, and this region showed an increase in the slope of the stress–strain curve

(Sultana & Wang, 2012). With the increasing C_0, the density of scaffolds increased and further resulted higher stress at lower strain.

Scaffold-I was prepared and stored in the saturated NaCl solution. When the saturated NaCl solution was diluted to a different concentration (C_{NaCl}) with water and scaffold-I was stored in these solutions for 48 h, E decreased from 4.0 kPa to 2.1 kPa, and P increased from 96.7% to 98.3% as the C_{NaCl} decreased (Fig. 3C) because of the decreasing salting-out effect. When the sample was transferred from the saturated NaCl to low-concentration NaCl, scaffold-I dissolved completely because that C_{NaCl} was insufficient to electronically screen the $-NH_3^+$.

During the freezing process, phase separation resulted in rearrangement of the polymer chains during construction of the interconnected pore network and the scaffold substrate layers by formation of hydrogen bonds between the polymer chains and water molecules (Nwe, Furuike, & Tamura, 2009). The temperature of the saturated NaCl solution was lower than the melting point of the frozen chitosan solution, and the interconnected pore network of the sample therefore remained, as shown in Fig. 2. Finally, intermolecular aggregations in scaffold-I served as junction points in the chain-entanglement network, which resulted in a scaffold with high elasticity (Fig. 3D) (Ladet, David, & Domard, 2008). The elastic recovery of scaffold-I indicated that the intermolecular aggregations were not destroyed during compression, which provided the basis for preparation of scaffold-II under compression.

3.4. Effect of preparation conditions on scaffold-II

Both the pH-dependent solubility of chitosan and the elastic recovery of scaffold-I were leveraged to fabricate scaffold-II. The Cl^- which was used to screen the $-NH_3^+$ was gradually replaced by OH^- in the NaOH solution, and the disappearance of ionic repulsion between the $-NH_3^+$ favoured physical junction points in the form of hydrogen bonding, hydrophobic interactions, and paracrystallite formation (Silva, Juenet, Meddahi-Pelle, & Letourneur, 2015; Wang et al., 2016). However, the initial concentration of the chitosan solution limited the structure and mechanical properties of the scaffold, making it difficult to fabricate a chitosan scaffold with high mechanical strength using this process.

Accordingly, a new compression step was used to densify the scaffold-I before treating in the NaOH solution. Under compression, junction points formed first between compacting molecule chains from the neutralization of NH_3^+ by OH^-, stabilising the structure and morphology of the compressive samples. Subsequently, the chain-entanglement points were disentangled as the Cl^- diffused to the NaOH solution, and the molecule chains were rearranged and synchronously form junction points. Finally, $-NH_3^+$ was completely neutralized to $-NH_2$ and a porous chitosan scaffold was prepared.

3.4.1. Compressive ratios (R value)

E increased and P decreased as the R value increased (Fig. 4A). At $R = 8$, E reached 520 kPa, which was nearly 100-fold higher than that
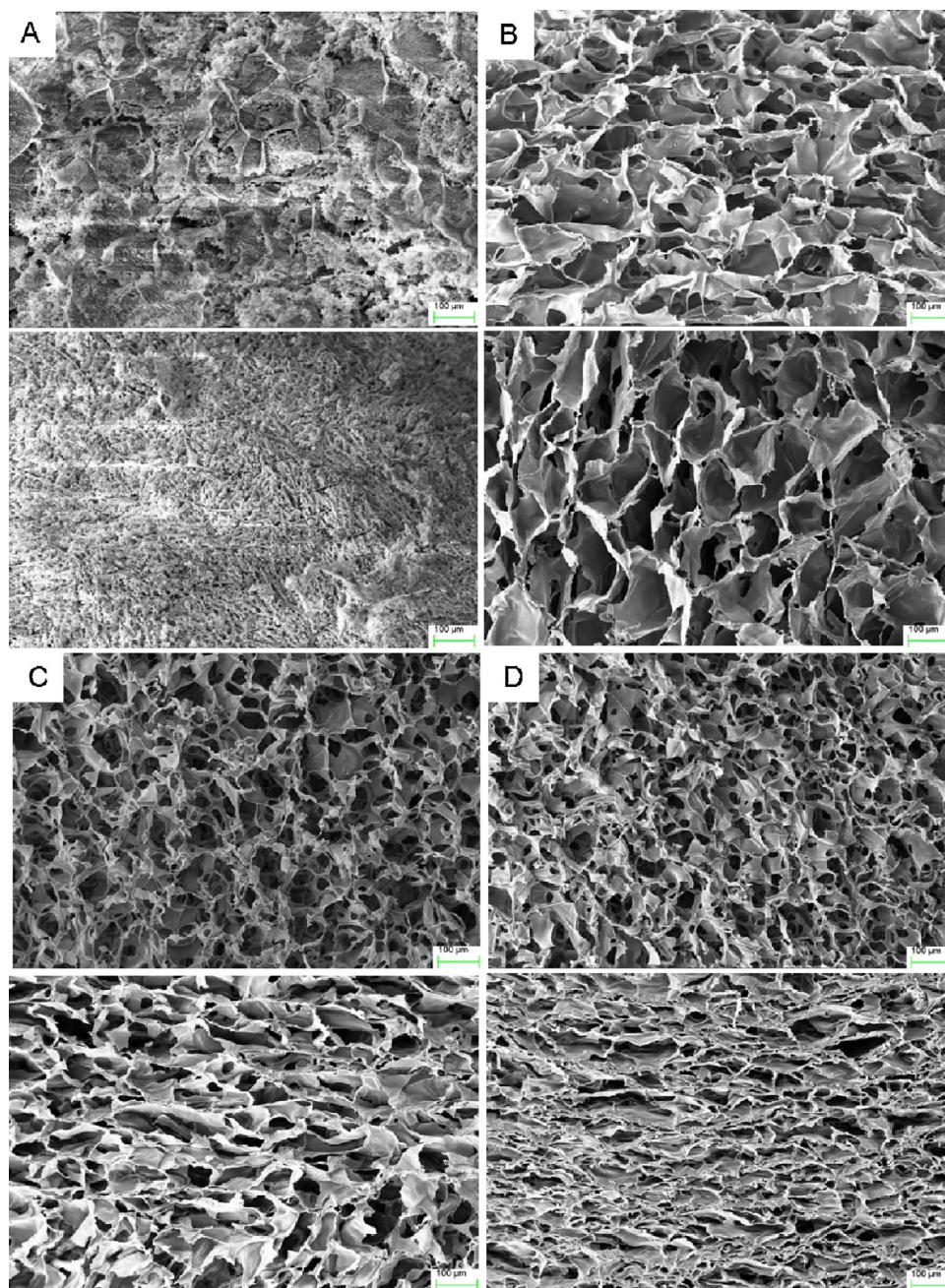
Fig. 2. SEM images of the scaffolds: (A) scaffold-I at 20 mg/ml; scaffold-II at different compressive ratios (*R*) (B) *R* = 1, (C) *R* = 3, (D) *R* = 6. Top: Section perpendicular to compression direction; Bottom: Section parallel to compression direction.

of initial samples (E_0 = 5.2 kPa, *R* = 1). Compression decreased the intermolecular distance and facilitated intermolecular interactions, and may be considered to concentrate the chitosan solution (Chen & Hwa, 1996). The increasing density of junction points improved the mechanical properties of the scaffold. Fig. 2 also shows that the pore size of scaffold-II decreased as *R* increased.

The stress–strain curves show that scaffold-II exhibited a linear relationship up to the strain point, and no obvious fracture behaviour was observed at any point during compression processing (Fig. 4B). Scaffold-II also possessed outstanding shape-recovery properties in 1 × PBS (Fig. 4C).

3.4.2. Concentration of NaOH solution

Fig. 5A illustrates that *E* increased slightly and *P* decreased slightly as the NaOH concentration (C_{NaOH}) increased for scaffold-II at *R* = 1 and *R* = 2. When the solution changed from NaOH solution to NaOH + NaCl solution, the properties of scaffold-II, with *R* = 1 and *R* = 2,

scarcely changed, as shown in Fig. 5B. This result can be interpreted by considering different contributions such as the change in the electrostatic potential during the neutralization inducing the formation of physical crosslinks, and ionic strength effects. The salting-out effect of NaCl in scaffold-I induces a screening of the electrostatic repulsions between polymer chains and should therefore favour physical junctions inside the scaffold (Ladet et al., 2008). The composition of neutralization solution (NaOH + NaCl) determines the kinetics of neutralization. Cl⁻ diffused out and OH⁻ diffused in the scaffold-I in neutralization solution. Nevertheless, the neutralization of OH⁻ only occurred after disassociation of Cl⁻. As a result, the dissociation of Cl⁻ screening determined the kinetics of neutralization and favoured physical junctions with little disentanglement. The structure of scaffold-I was mainly retained in scaffold-I at all values of C_{NaOH}. Figs. 1 and 2 also confirmed this result.
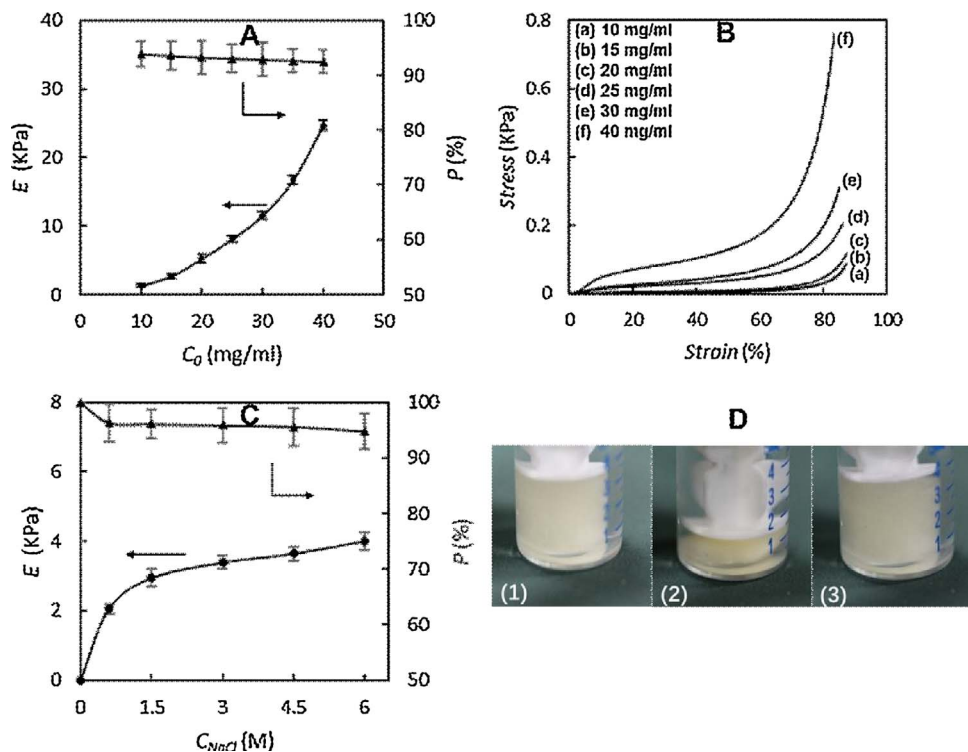
Fig. 3. The properties of scaffld-I. (1) Different original chitosan concentration (C_0): (A) compressive elastic modulus (E) and porosity (P), (B) compressive stress–strain curve and (2) $C_0 = 20$ mg/ml: (C) E and P with different NaCl solutions (C_{NaCl}), (D) shape recovery in NaCl solution ($C_{NaCl} = 3$ M).

3.4.3. The original concentration of the chitosan solution

The effect of the C_0 of the chitosan solution on E and P of scaffold-II was also investigated. As C_0 increased from 10 mg/ml to 40 mg/ml, E increased from 1.34 kPa to 24.7 kPa, and the porosity decreased from 94.8% to 92.5% (Fig. 6). This was consistent with the effect of R and confirmed that the increasing density of junction points from the high C_0 also resulted to the excellent mechanical properties of the scaffold. For the sample prepared using 20 mg/ml, the compressive stress–strain curve was similar to that of scaffold-I except that scaffold-II had a higher stress than scaffold-I at the same strain.

3.4.4. pH-responsive properties

As shown in Fig. 7, almost no change was observed in basic solutions containing $1\times$ PBS (pH = 7.4 and 9.0). In acidic solutions containing $1\times$ PBS (pH = 3.0 and 5.0), scaffold-II gradually dissolved, and the samples with a higher R dissolved more slowly. Conversion between $-NH_3^+$ and $-NH_2$ is a reversible chemical reaction. Consequently, scaffold-II gradually dissolves in an acidic environment, and this pH-responsive property could be used in tissue engineering and drug release. The diffusion rate of H^+ inside the samples regulated the dissolution rate. Consequently, samples with a higher R value had a lower
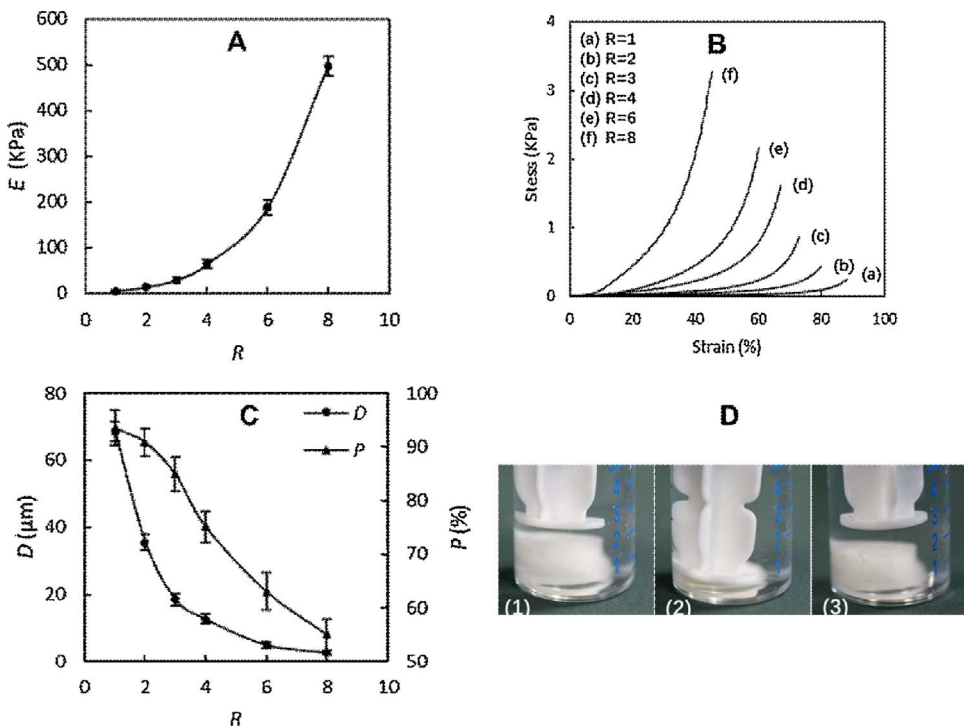

Fig. 4. The properties of scaffold-II at different compressive ratios (R): (A) compressive elastic modulus (E); (B) compressive stress-strain curve; (C) average pore diameter (D) and porosity (P); (D) shape recovery of sample in $1\times$ PBS (pH = 7.4) at $R = 2$.
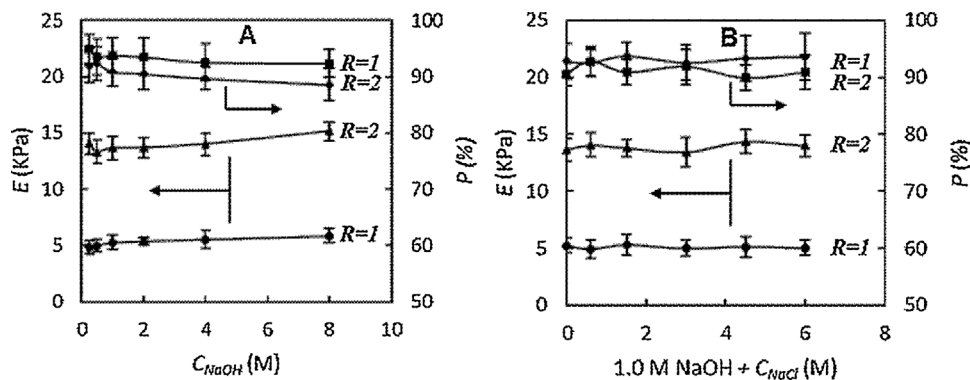
Fig. 5. The effects of C_{NaOH} on the compressive elastic modulus (E) and porosity (P) of scaffold-II: (a) $R = 1$ and (b) $R = 2$.

pH-response rate.

3.4.5. In vitro cytotoxicity

The cytotoxicity of the chitosan scaffold was determined using an MTT assay. As illustrated in Fig. 8, all the samples demonstrated cytocompatibility for fibroblast cells. These findings are consistent with previous research results (Ladet et al., 2008; Li et al., 2014).

3.4.6. Cell behaviour of hASCs

Cell adhesion onto the scaffolds was assessed by confocal microscopy (Fig. 9). The images indicated that cells could adhere to the fibres of the chitosan scaffolds after 24 h of culture, regardless of E or P. Due to the high porosity and pore interconnectivity of these scaffolds, cell adhesion was not confined to the surface and cells could migrate into the scaffolds. Nevertheless, the number of human adipose-derived stem cells (hASCs) adhering to the scaffolds increased as R increased, because the density of the chitosan fibres increased.

According to the formation mechanism of scaffold-I and scaffold-II, NaCl could be further replaced by other monovalent anionic salts with a sufficiently high concentration to electronically screen the -NH_3^+, and the NaOH could be replaced by other bases to neutralize −NH_3^+ to −NH_2. In our previous study, PBS was used to prepare the chitosan scaffold to prevent the strong bases from damaging the bioactive factors or the drug payload (Xu, Han, & Lin, 2017). This study also showed that NH_4OH, KOH, $Ca(OH)_2$, or $20\times$ PBS was sufficient to convert scaffold-I to scaffold-II.

4. Conclusions

In summary, a novel compression method was developed to fabricate chitosan scaffolds with tuneable mechanical properties and topography. This method overcame the low solubility and high viscosity of the polysaccharide solution, permitting adjustment of the structure and properties of the scaffold to adapt to the requirements of different tissues. Furthermore, because no cross-linker was introduced, undesirable
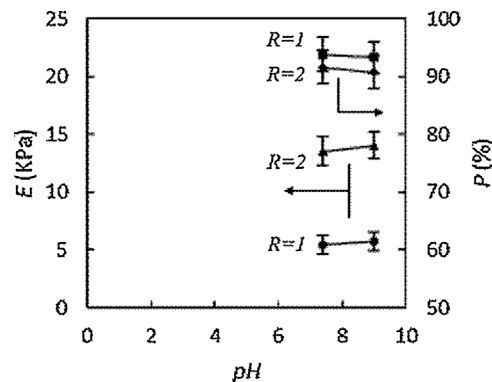

Fig. 7. pH-responsive properties, compressive elastic modulus (E) and porosity (P), of scaffold-II with $R = 1$ and $R = 2$ in $1\times$ PBS (pH = 3.0, 5.0, 7.4 and 9.0).
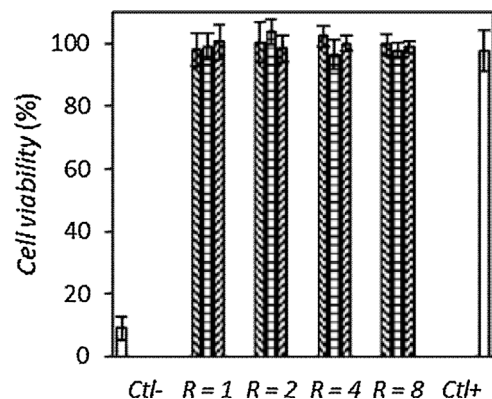

Fig. 8. Viability of L929 fibroblasts exposed to extracts during incubation with various scaffolds with R = 1, 2, 4, and 8 at different concentrations (0.5, 1.0 and 1.5 mg/ml). Ctl−, 10% DMSO; Ctl+, medium culture.
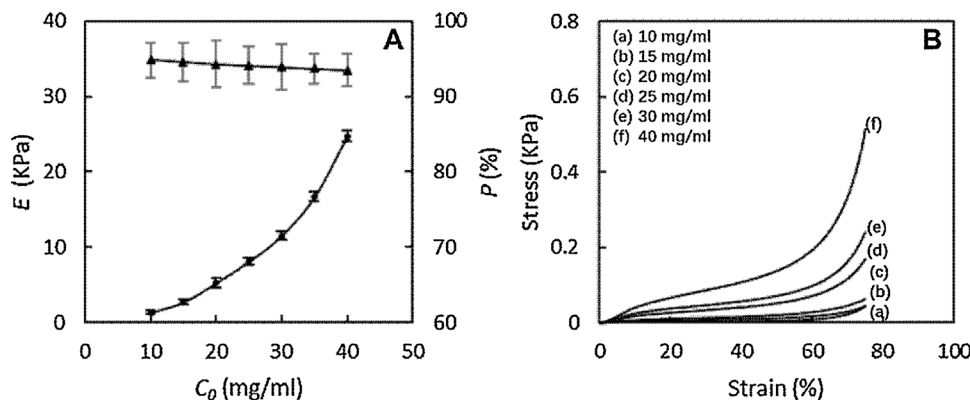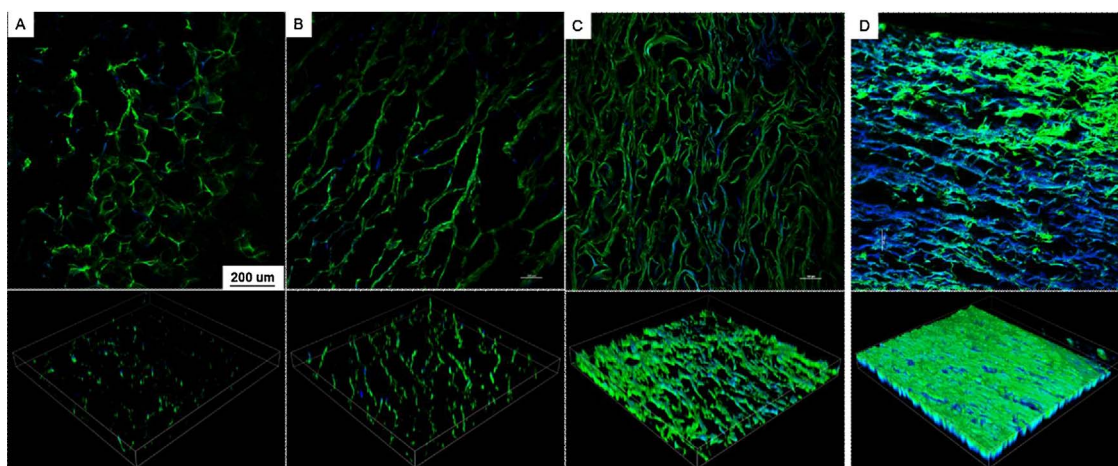

Fig. 6. The properties of scaffold-II at different initial concentrations (C_0): (A) compressive elastic modulus (E) and porosity (P); (B) compressive stress–strain curve.

Fig. 9. Confocal micrographs of human adipose-derived stem cells (hASCs) on chitosan scaffolds formed using different compression ratios: (A) $R = 1$, (B) $R = 2$, (C) $R = 4$, (D) $R = 8$ after 24 h of culture. FITC-phalloidin is shown in green and nuclei are shown in blue, following staining with DAPI. The chitosan fibres are also shown in green, due to the auto-fluorescence signal of chitosan. (For interpretation of the references to colour in this figure legend, the reader is referred to the web version of this article.)

alteration of the biological properties of the chitosan scaffold was avoided. Because it does not require sophisticated instrumentation, this method could easily be scaled up for commercial applications. In addition, it could be expanded for use in fabricating elastic scaffolds with secondary chemical reaction, facilitating fabrication of scaffolds with tuneable structure and properties.

Acknowledgement

References

Albanna, M. Z., Bou-Akl, T. H., Blowytsky, O., & Matthew, H. W. (2012). Chitosan fibers with improved biological and mechanical properties for tissue engineering applications. *Journal of the Mechanical Behavior of Biomedical Materials, 20*(4), 217–226.

Bhattarai, N., Gunn, J., & Zhang, M. Q. (2010). Chitosan-based hydrogels for controlled, localized drug delivery. *Advanced Drug Delivery Reviews, 62*(1), 83–99.

Campbell, T. D., Wiesmann, W. P., & McCarthy, S. J. (2012). Method for preparing a compressed wound dressing. *HemCon Medical Technologies Inc.* US 8313474.

Chen, R. H., & Hwa, H. D. (1996). Effect of molecular weight of chitosan with the same degree of deacetylation on the thermal, mechanical, and permeability properties of the prepared membrane. *Carbohydrate Polymers, 29*(4), 353–358.

Choi, S.-W., Xie, J., & Xia, Y. (2009). Chitosan-based inverse opals: Three-dimensional scaffolds with uniform pore structures for cell culture. *Advanced Materials, 21*(29), 2997–3001.

Farrugia, B. L., Whitelock, J. M., Jung, M., McGrath, B., O'Grady, R. L., McCarthy, S. J., et al. (2014). The localisation of inflammatory cells and expression of associated proteoglycans in response to implanted chitosan. *Biomaterials, 35*(5), 1462–1477.

Geng, L., Feng, W., Hutmacher, D. W., Wong, Y. S., Loh, H. T., & Fuh, J. Y. H. (2005). Direct writing of chitosan scaffolds using a robotic system. *Rapid Prototyping Journal, 11*(2), 90–97.

Huang, Y., Onyeri, S., Siewe, M., Moshfeghian, A., & Madihally, S. V. (2005). In vitro characterization of chitosan-gelatin scaffolds for tissue engineering. *Biomaterials, 26*(36), 7616–7627.

Hutmacher, D. W. (2000). Scaffolds in tissue engineering bone and cartilage. *Biomaterials, 21*(24), 2529–2543.

Jana, S., Florczyk, S. J., Leung, M., & Zhang, M. (2012). High-strength pristine porous chitosan scaffolds for tissue engineering. *Journal of Materials Chemistry, 22*(13), 6291–6299.

Khan, F., & Ahmad, S. R. (2013). Polysaccharides and their derivatives for versatile tissue engineering application. *Macromolecular Bioscience, 13*(4), 395–421.

Ladet, S., David, L., & Domard, A. (2008). Multi-membrane hydrogels. *Nature, 452*(7183), 76–79.

Langer, R., & Vacanti, J. P. (1993). Tissue engineering. *Science, 260*(5110), 920–926.

Li, G., Zhao, X., Zhao, W., Zhang, L., Wang, C., Jiang, M., et al. (2014). Porous chitosan scaffolds with surface micropatterning and inner porosity and their effects on Schwann cells. *Biomaterials, 35*(30), 8503–8513.

Ma, P. X. (2004). Scaffolds for tissue fabrication. *Materials Today, 7*(5), 30–40.

Madihally, S. V., & Matthew, H. W. T. (1999). Porous chitosan scaffolds for tissue engineering. *Biomaterials, 20*(12), 1133–1142.

Nwe, N., Furuike, T., & Tamura, H. (2009). The mechanical and biological properties of chitosan scaffolds for tissue regeneration templates are significantly enhanced by chitosan from *Gongronella butleri. Materials, 2*(2), 374–398.

O'Brien, F. J. (2011). Biomaterials & scaffolds for tissue engineering. *Materials Today, 14*(3), 88–95.

Oh, H. H., Ko, Y.-G., Lu, H., Kawazoe, N., & Chen, G. (2012). Preparation of porous collagen scaffolds with micropatterned structures. *Advanced Materials, 24*(31), 4311–4316.

Sadeghi, D., Karbasi, S., Razavi, S., Mohammadi, S., Shokrgozar, M. A., & Bonakdar, S. (2016). Electrospun poly(hydroxybutyrate)/chitosan blend fibrous scaffolds for cartilage tissue engineering. *Journal of Applied Polymer Science, 133*(47), 9–14.

Silva, A. K. A., Juenet, M., Meddahi-Pelle, A., & Letourneur, D. (2015). Polysaccharide-based strategies for heart tissue engineering. *Carbohydrate Polymers, 116*, 267–277.

Subramanian, A., & Lin, H. Y. (2005). Crosslinked chitosan: Its physical properties and the effects of matrix stiffness on chondrocyte cell morphology and proliferation. *Journal of Biomedical Materials Research A, 75A*(3), 742–753.

Sultana, N., & Wang, M. (2012). PHBV/PLLA-based composite scaffolds fabricated using an emulsion freezing/freeze–drying technique for bone tissue engineering: Surface modification and in vitro biological evaluation. *Biofabrication, 4*(1), 015003.

Sun, Y., Li, Y., Nie, J., Wang, Z., & Qiao ling, H. U. (2013). High-strength chitosan hydrogels prepared from LiOH/urea solvent system. *Chemistry Letters, 42*(8), 838–840.

Wang, Z., Nie, J., Qin, W., Hu, Q., & Tang, B. Z. (2016). Gelation process visualized by aggregation-induced emission fluorogens. *Nature Communications, 7*, 12033.

Xu, Y., Han, J., & Lin, H. (2017). Fabrication and characterization of a self-crosslinking chitosan hydrogel under mild conditions without the use of strong bases. *Carbohydrate Polymers, 156*, 372–379.

Yang, Y., Wang, X., Yang, F., Shen, H., & Wu, D. (2016). A universal soaking strategy to convert composite hydrogels into extremely tough and rapidly recoverable double-network hydrogels. *Advanced Materials, 28*(33), 7178–7184.

Zhang, Y. Z., Venugopal, J. R., El-Turki, A., Ramakrishna, S., Su, B., & Lim, C. T. (2008). Electrospun biomimetic nanocomposite nanofibers of hydroxyapatite/chitosan for bone tissue engineering. *Biomaterials, 29*(32), 4314–4322.